ISSN 0036-0236, Russian Journal of Inorganic Chemistry, 2021, Vol. 66, No. 14, pp. 2091–2104. © Pleiades Publishing, Ltd., 2021.

THEORETICAL
INORGANIC CHEMISTRY

Application of Group Theory for Evaluating the Jahn–Teller Effect and Analyzing the Stability Structure of Boron $\left(B_{n\,=\,(3-7)}^{\mp,0}\right)$ Clusters

M. Monajjemi*

Department of Chemical Engineering, Central Tehran Branch, Islamic Azad University, Tehran, 1496969191 Iran
**e-mail: Maj.monajjemi@iauctb.ac.ir*

Received April 9, 2021; revised June 21, 2021; accepted June 30, 2021

Abstract—The second order Jahn–Teller effects (SOJT) can be occurring during interactions among filled and empty MOs of the similar symmetries. By this work, for some of the $B_n^{\mp,0}$ clusters the diatropic current (aromatic) and for some others paratropic current (anti-aromatic) have been predicted some of theme presented planar or quasi-planar structures due to Jahn–Teller and pseudo Jahn-teller effects. Via this effort, it has been exhibited that the aromaticity or anti-aromaticity can be assigned based on the $4n + 2$ (or $4n$) electron counting rule for either π- or σ-electrons in the planar structures. In addition, planarity and non-planarity of those clusters in viewpoint of Jahn–Teller and pseudo Jahn–Teller effect have been discussed in terms of delocalization and aromaticity. Via application of group theory, it has been exhibited that Jahn-Teller distorted structures of $B_n^{\mp,0}$ clusters belonging to the C_n, C_{nv}, C_{nh}, D_n, D_{nh} for $n > 2$, and D_{nd} and S_{2n} for $n > 1$ point groups are anti-aromatic.

Keywords: B_n clusters, Jahn–Teller effect, pseudo-Jahn–Teller effect, aromaticity

DOI: 10.1134/S0036023621140035

INTRODUCTION

Berger [1] exhibited that a general symmetry fundamental for antiaromaticity is known as first-order and second-order Jahn–Teller distorted systems. In other concept, antiaromaticity appears because of the first-order Jahn-Teller effect and geometric distortions leading to make up islands of aromaticity, low atomization energy, low first singlet vertical excitation energy, NICS values close to zero or positive [2–7]. Second order Jahn–Teller effects (SOJT) occur during interactions among filled and empty molecular orbitals of the similar symmetries. These interactions generally lead to conformational distortion that extent is against proportional to the energy differences among the orbitals [4–9]. In inorganic chemistry, a vast importance of molecules and ions can be presented via a single the classical molecules (Lewis structures) with either multiple 2-center & 2-electron bonds and with a suitable number of lone pairs of electron rich atoms. Chemical bonding in several inorganic structures also can be presented via Lewis structure, but usually in inorganic chemistry problems. If, however, the Lewis structure descriptions are not enough, then the resonances of Lewis forms are used. The major advantages of those mentioned chemical bonding models are that we can predict possible isomers of classical molecules using just paper and pencil and with high certainty we also can predict which isomers can be more stable one compared to a given stoichiometry [7, 8]. Although, there are no chemical bonding models allowing us for using the approach for predicting isomers of homo-atomic and hetero-atomic structures, the ab initio techniques can help us for finding global situation of these clusters as well as their low-lying isomers. Pioneering study on $B_n^{\mp,0}$ ions have been accomplished and investigated with several researchers [9–21]. As instance they produced boron clusters ions through molecular beams using laser vaporization to study their chemical reactions and chemical physics properties [22–28] and designed the 3D structures for $B_n^{\mp,0}$ clusters. Consequently, quantum ab initio estimation has confirmed that boron clusters prefer planar or quasi-planar structures related to Jahn–Teller & pseudo-Jahn–Teller effects [29–33]. Although these kind computational investigations were not confirmed experimentally, in some recent studies experimental works has been measured spectrophotometry for several $B_n^{\mp,0}$ clusters such as: $B_3^+(D_{3h})$, $B_3^-(D_{3h})$, B_4 (D_{2h}), $B_5^+(D_{5h})$, $B_5^-(C_{2V})$ $B_6^-(D_{2h})$, $B_6^+(D_{6h})$, $B_6^0(C_{5V})$, $B_7^+(C_{6V})$, $B_7^-(C_{2V})$ $B_9^-(D_{8h})$ and $B_{10}^0(C_{2h})$ neutrals and ions [34–40]. The structures of those ions have been discussed computationally and confirmed via comparisons of experimental photoelectron spectrophotometry. These studies have been verified the 2D or quasi 2D

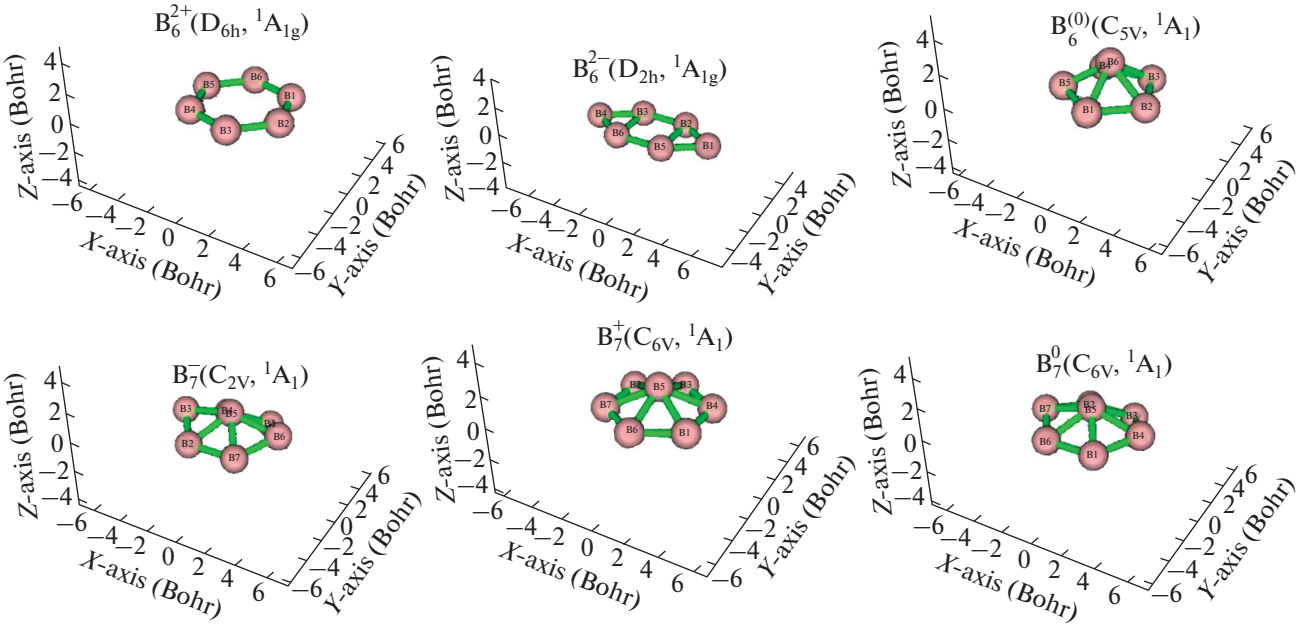

Fig. 1. Global minimum structures of a few structures of $B_n^{\mp,0}$ (n = 3–6) based on DFTB+/cc-PVDZ level of theory.

structures in many of them. Planarity and non-planarity of these clusters in viewpoint of Jahn–Teller & pseudo-Jahn–Teller effect have been discussed in terms of delocalization [39–42] and aromaticity [3, 5, 21]. High symmetric planar boron clusters B_3^- (D_{3h}), B_4 (D_{4h}) are corresponded to the "$4n + 2$" Huckel rule and might be considered as aromatic clusters. Boron clusters with $4n$-electrons such as B_6^{2-} (4π electrons) is discussable as anti-aromatic.

Aihara performed analysis of aromaticity of boron clusters $B_n^{0,\mp1,\mp2}$ (n = 3–10) in viewpoint of conformational resonance energy (CRE) and discussed that all B_n clusters are largely-aromatic including systems with $4n$ electrons [43, 44]. For resolving the conflict about aromaticity or antiaromaticity of closed shell boron clusters, we calculated a wide chemical physics analyzing in the pure B_n clusters $B_n^{0,\mp1,\mp2}$ (n = 3–10). The penetration of σ-electrons on geometry of B_n clusters in viewpoint of Jahn–Teller & pseudo-Jahn–Teller has not been discussed yet.

RESULTS

Jahn–Teller (Sojt) Approach for $B_{n=(3-7)}^{\mp,0}$

Geometry optimization and also frequency calculation has been done for the $B_n^{0,\mp1,\mp2}$(n = 3–0) homocyclic series with method of density functional theory (DFTB, DFTB+ and CAM-B3LYP) including the cc-pVTZ, EPR-III basis sets. The optimized structures are exhibited in Fig. 1. Natural bond orbitals (NBO), electron localized function (ELF) and localized orbital localization (LOL) were analyzed via Multifunctional Wave function Analyzer [45]. All calculation has been performed using Gaussian 09 program and pictures were made using the chem3D program.

$B_3^{0,\mp1}$ clusters. B_3^+ is a complete structure in the closed shell ground state in viewpoint of spectrophotometry experimental studies with orbitals as D_{3h} ($^1A_1'$): ($1a_1'^2$,$1e'^4$,$1a_2''^2$) [39–42] (Fig. 1). MOs of 4 valances indicate that the HOMO ($1a_2''^2$) is an π orbital from overlapping of $2P_z$ located in three atoms of B atoms. The other set of valance orbitals including HOMO-1 ($1e'^4$) and HOMO-2 ($1a_1'^2$) formed into three $2c$–$2e$ of B–B bonds with the occupation numbers 1.69 and the powerful s–p hybridization in the B_3^+ cation ($0.7SP^{1.20}$) (Table 1) is accountable for bonding behavior of the lowest 3 valence MOs.

Two electrons of π-HOMO provides π-MO aromatic situation due to $4n$ + 2 Huckel rule (n = 0). Three other molecular orbitals make $2c$–$2e$ bonds, even though their occupation numbers (1.88) are slightly smaller than 2.00 in a classical $2c$–$2e$ bonds. In B_3^- the pair electrons occupies $2a_1'^2$, where is σ-MO from overlapping of the $2p$ AOs. Two electrons of delocalized σ-HOMO provides σ-Aromatic and doubly occupied π-HOMO-1 is responsible for π-aromaticity in B_3^- and also

Table 1. Natural bond orbitals of $B_n^{0,\mp1}$ clusters based on DFTB+/cc-PVDZ level of theory

NBO	Bond length	Occupancy	Energy	Coefficients/Hybrids
		B_3^-		
1.BD(1) B1–B2	1.570	1.8827	–0.10597	$0.7SP^{1.42} + 0.7SP^{1.42}$
2.BD(1) B1–B3	1.570	1.8827	–0.10599	$0.7SP^{1.42} + 0.7SP^{1.42}$
3.BD(1) B2–B3	1.570	1.8827	–0.10599	$0.7SP^{1.42} + 0.7SP^{1.42}$
		B_3^+		
1.BD(1) B1–B2	1.380	1.69780	–0.70228	$0.7SP^{1.20} + 0.7SP^{1.20}$
2.BD(1) B1–B3	1.380	1.69779	–0.70227	$0.7SP^{1.20} + 0.7SP^{1.20}$
3.BD(1) B2–B3	1.380	1.69779	–0.70227	$0.7SP^{1.20} + 0.7SP^{1.20}$
		B_4^{2-}		
1.BD(1) B1–B2	1.657	0.97448	0.00533	$0.6SP^{1.93} + 0.7SP^{1.11}$
2.BD(1) B2–B3	1.657	0.89941	0.28966	$0.7SP^{18} + 0.7SP^{18}$
3.BD(1) B3–B4	1.657	0.97448	0.00534	$0.7SP^{1.11} + 0.6SP^{1.93}$
4.BD(1) B4–B1	1.657	0.89941	0.28966	$0.7SP^{18} + 0.7SP^{18}$
		B_4^{2+}		
1.BD(1) B1–B2	1.590	1.89741	–0.96930	$0.7SP^{1.19} + 0.7SP^{1.19}$
2.BD(1) B2–B3	1.590	1.89741	–0.96930	$0.7SP^{1.19} + 0.7SP^{1.19}$
3.BD(1) B3–B4	1.590	1.89741	–0.96930	$0.7SP^{1.19} + 0.7SP^{1.19}$
4.BD(1) B4–B1	1.590	1.89741	–0.96930	$0.7SP^{1.19} + 0.7SP^{1.19}$
		B_5^+		
1.BD(1) B1–B2	1.643	1.96657	–0.71414	$0.7SP^{1.01} + 0.7SP^{1.01}$
2.BD(1) B2–B3	1.643	1.96649	–0.71414	$0.7SP^{1.01} + 0.7SP^{1.01}$
3.BD(1) B3–B4	1.643	1.96653	–0.71414	$0.7SP^{1.01} + 0.7SP^{1.01}$
4.BD(1) B4–B5	1.643	1.96654	–0.71415	$0.7SP^{1.01} + 0.7SP^{1.01}$
5.BD(1) B5–B1	1.643	1.96648	–0.71413	$0.7SP^{1.01} + 0.7SP^{1.01}$
		B_5^-		
1.BD(1) B1–B2	1.607	0.90066	–0.20704	$0.6SP^{2.18} + 0.8SP^{1.51}$
2.BD(1) B2–B3	1.607	0.90067	–0.20705	$0.6SP^{1.51} + 0.8SP^{2.18}$
3.BD(1) B3–B4	1.558	0.95540	–0.19551	$0.6SP^{2.80} + 0.8SP^{1.15}$
4.BD(1) B4–B5	1.591	0.97929	–0.25457	$0.7SP^{1.12} + 0.7SP^{1.12}$
5.BD(1) B5–B1	1.558	0.95542	–0.19554	$0.6SP^{2.80} + 0.8SP^{1.15}$
		B_6^{2-}		
1.BD(1) B1–B2	1.534	1.8895	–0.01439	$0.7SP^{1.11} + 0.7SP^{1.11}$
2.BD(1) B2–B3	1.677	1.9832	–0.06301	$0.7SP^{1.48} + 0.7\ SP^{1.48}$
3.BD(1) B3–B4	1.534	1.8895	–0.01439	$0.72SP^{1.61} + 0.7SP^{1.11}$
4.BD(1) B4–B5	1.534	1.8895	–0.01439	
5.BD(1) B5–B6	1.677	1.9832	–0.06301	$0.7SP^{1.48} + 0.7SP^{1.48}$
6.BD(1) B6–B1	1.534	1.8895	–0.01439	

Table 1. (Contd.)

NBO	Bond length	Occupancy	Energy	Coefficients/Hybrids
		B_6^{2+}		
1.BD(1) B1–B2	1.583	1.98008	–0.95008	$0.7SP^{1.05}$ $0.707\ SP^{1.05}$
2.BD(1) B2–B3	1.583	1.98009	–0.95008	$0.7SP^{1.05} + 0.7SP^{1.05}$
3.BD(1) B3–B4	1.583	1.98010	–0.95009	$0.7SP^{1.05} + 0.7\ SP^{1.05}$
4.BD(1) B4–B5	1.583	1.98008	–0.95008	$0.7SP^{1.05}$ $0.707\ SP^{1.05}$
5.BD(1) B5–B6	1.583	1.98009	–0.95008	$0.7SP^{1.05}$ $0.707\ SP^{1.05}$
6.BD(1) B6–B1	1.583	1.98010	–0.95009	$0.7SP^{1.05} + 0.7\ SP^{1.05}$
		B_6^0		
1.BD(1) B1–B2	1.681	1.92924	–0.40651	$0.7SP^{1.02} + 0.7\ SP^{1.58}$
2.BD(1) B2–B3	1.681	1.92919	–0.40650	$0.7S\ P^{1.37} + 0.7SP^{1.37}$
3.BD(1) B3–B4	1.681	1.92956	–0.41245	$0.7SP^{1.58} + 0.7\ SP^{1.02}$
4.BD(1) B4–B5	1.681	1.92918	–0.40649	$0.7SP^{1.27} + 0.7\ SP^{1.43}$
5.BD(1) B5–B6	1.704	1.49834	–0.32582	$0.7SP^{1.36} + 0.7\ SP^{1.36}$
6.BD(1) B6–B1	1.704	1.50932	–0.35668	$0.\ 6S\ P^{7.3} + 0.8S\ P^{1.14}$

Table 2. Gap energies and various HOMO-n (n = 1, 2 and 3) energies

Molecule	LUMO/HOMO Gap, kJ/mol	HOMO, Hartree	HOMO-1, Hartree	HOMO-2, Hartree	HOMO-3, Hartree	HOMO//HOMO-1 overlapping	HOMO//LUMO overlapping
$B_6^{(2-)}$	219.30	–0.20625	–0.18262	–0.16473	–0.13341	0.595	0.557
$B_6^{(2+)}$	303.84	–0.67886	–0.69083	–0.75810	–0.82249	0.633	0.574
B_6^0	150.40	–0.23475	–0.23478	–0.29181	–0.32987	0.576	0.632
B_5^-	216.02	0.03019	–0.02475	–0.05201	–0.05357	0.650	0.639
B_5^+	379.77	–0.46932	–0.48320	–0.55687	–0.55687	0.619	0.624
B_5^0	142.59	–0.15759	–0.24764	–0.26894	–0.32218	0.621	0.654
$B_4^{(2-)}$	192.44	0.31949	0.24676	0.20523	0.20157	0.874	0.760
$B_4^{(2+)}$	224.61	–0.76785	–0.79981	–0.91352	–0.91352	0.618	0.621
B_3^-	332.09	0.02218	–0.00384	–0.06875	–0.06876	0.613	0.826
B_3^+	225.68	–0.53188	–0.60101	–0.60101	–0.91303		

($1a_1'^2$) HOMO-3, ($1e'^4$) HOMO-2 are transformed into $2c$–$2e$ of B–B bonds (Table 2). Therefore B_3^- is a doubly σ–π aromatic system and occupation numbers 1.88 with powerful s–p hybridization in the B_3^- cation ($0.7SP^{1.42}$) (Table 1). This property of doubly aromatic behavior is also confirmed the symmetry of first singlet excitation energy. In addition, D_{3h} systems including a doublet ground vibrionic level, in the dipole approximation, the IR transitions from ground state "E" to excited state are allowed, due to $E \otimes E = (A_1 + A_2 + E)$.

$B_4^{0,-2}$ clusters. Electronic and geometry structures of neutral B_4^0 was clearly explained [35] as D_{2h} (^1A_g) global optimum geometry including a distortion due to pseudo Jahn–Teller effect (PJTE). MOs of B_4^0 with D_{2h} (^1A_g) point groups are $1a_g^2$, $1b_{1u}^2$, $1b_{2u}^2$, $1b_{3g}^2$, $1b_{3u}^2$, $2a_g^2$. These orbitals can be localized into four classical

peripheral $2c$–$2e$ B–B bonds are HOMO-2 ($1b_{3g}^2$), HOMO-3 ($1b_{2u}^2$), HOMO-4 ($1b_{1u}^2$) and HOMO-5($1a_g^2$) and also are the lowest 4 MOs. In excited states, i.e., degenerate E_g and E_u and non-degenerate B_{2g} are located between the A_{1g} ground and B_{2u} excited states. The PJTE ($^1A_{1g} + {}^1B_{2u}$) $\otimes$ b_{2u} occurs for the B_4^0 due to mixing of the A_{1g} ground and B_{2u} excited states, and other excited states that are lower than B_{2u} do not contribute to the PJTE problem. Due to nature of this distortion, the barrier for ''squareness'' is small and even at medium temperature, B_4^0 is square.

In other hand the tight s–p-hybridization on the both boron atoms: (from HOMO-2 through HOMO-5) is related for the formation of four classical B–B bonds. Two other MOs which are delocalized, contribute in the global bonding and NBO analysis exhibit eight lone pairs with the occupation number 0.5 e on each boron atoms (Table 2).

Remain orbital ($1b_{3u}^2$) which belong to the HOMO-1 is perfectly bonding that is built via overlapping of $2p_z$ atomic orbitals in out of plane to make the cluster–aromatic. $2a_g^2$ is HOMO organized through overlapping among $2p$ atomic orbitals thus this structure can be characterized as doubly aromatic system [21]. B_4^{2-}, has a planar structure with D_{4h} ($^1A_{1g}$) point groups are $1a_{1g}^2$, $1e_u^4$, $1b_{1g}^2$, $1b_{2g}^2$, $2a_{1g}^2$, $1a_{2u}^2$ the iso-electronic & iso-structural B_4^{2-} is also doubly aromatic (σ &π) molecule with 4 "$2c$–$2e$" peripheral B–B bonds and its aromaticity has been confirmed through the ring-current susceptibility by Sundholm and coworkers [9]. In $B_4^{2-} \rightarrow B_4 + 2e^-$symmetry reduction, it is notable that B_4^{2-} Molecule has a square-planar geometry in the high-symmetry configuration with a doubly degenerate ^2E_g term resulting in a JT E $\otimes$ ($b_1 + b_2$) problem which the possible JT and PJT distortions of this system is exhibited in Scheme 1.

JT-coordinates are of either b_{1g} or b_{2g} symmetry, resulting in D_{2h} configurations of a rhombus or rectangle, respectively that are not ultimate situation due to the PJTE, therefore may produce further distortions such as B_4 with D_{2h} configuration. Especially in a strong vibrionic coupling of $^2B_{3g}$ (ground state) to $^2B_{3u}$ (excited state) of the rectangular configuration, an Au-kind distortion is done ($^2B_{3g} \times B_{3u} = Au$).

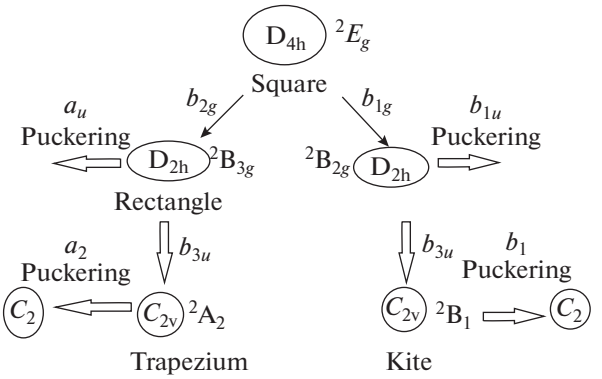

Scheme 1. Possible JT and PJT distortions of a B_4^{2-} in an electronic ^2E_g state.

Same as that a puckering of the rhombus (b_{1u} distortion) can be done via strong pseudo JT coupling towards its $^2A_{2u}$ excited state. In addition, PJT coupling to the other $^2A_{1u}$ state is strong and the distortion b_{3u} leads to a trapezium configuration that is a puckering situation due to the excited state of $^2A_1$. The rhombus can also be distorted to a kite situation (Scheme 1) and the latter may be puckered by the PJT $B_1 \times A_1$ vibrionic coupling. The energy differences between B_4^{2-} and B_4^0 configurations are small. So, a tight and high level calculation including correlation terms is needed to reveal the real minima and saddle points. The best results show that the puckered rhombus gives the absolute minimum energy, while the planar rectangle is also a minimum, which is 2.6 kcal/mol higher in energy than the puckered rhombus. $B_5^{0\mp1}$: B_5^+, belongs to the C_{2v} structure that somewhat is distorted in its planar pentagon (Fig. 1). Our calculations indicated that the D_{5h} ($^1A_1'$:: ($^1A_1'$: $1a_1'^2$, $1e_1'^4$, $1e_2'^4$, $1a_2''^2$, $2a_1'^2$) planar pentagon has two imaginary frequencies at the B3LYP/cc-pvTZ method and basis set and in the global minimum, C_{2v} ($^1A_1$:$1a_1^2$, $1b_2^2$, $2a_1^2$, $3a_1^2$, $1b_1^2$, $2b_2^2$, $4a_1^2$, $3b_2^2$) structure boron bonds a little bit distorted due to the second order Jahn–Teller Effect (Table 3).

According to our calculation (CCSD (T)/6-311+G*), the global minimum C_{2v} ($^1A_1$) structure (Fig. 1) is 0.36 kcal/mol smaller than the saddle point D_{5h} ($^1A_1'$) and via a ZPE correction (harmonic frequencies at CCSD (T)/6-311+G*) and the vibrational of D_{5h}($^1A_1'$) the structure around 0.011 kcal/mol (Table 3) is smaller than the vibrational of C_{2v} ($^1A_1$). The planar pentagonal of B_5^+ can also be explained from NBO analysis. By these analyzing the HOMO-2 and HOMO-2' ($1e_2'^4$), HOMO-3 and HOMO-3' ($1e_1'^4$), and HOMO-4 ($1a_1'^2$) might be localized into five peripheral

Table 3. Electronic properties of $B_n^{\mp,0}$ ($n = 3$–6) in ground and exited states

State	Configuration, ground state	Point group	First singlet vertical excitation energy, eV	Totally delocalized	
				π-MO$_s$	σ-MO$_s$
$B_6^{(2-)}$	^1A_g: $1a_g^2, 1b_{1u}^2, 2a_g^2, 1b_{2u}^2, 1b_{3g}^2, 1b_{3u}^2, 3a_g^2, 2b_{2u}^2, 2b_{1u}^2, 1b_{2g}^2$)	D_{2h}	0.86	2	2
B_6^0	$^1A_1$: $1a_1^2, 1e_1^4, 2a_1^2, 1e_2^4, 3a_1^2, 2e_1^4$	C_{5V}	2.31	1	3
B_5^-	$^1A_1$: $1a_1^2, 1b_2^2, 2a_1^2, 3a_1^2, 1b_1^2, 2b_2^2, 4a_1^2, 1a_2^2$	C_{2v}	1.12	1	2
B_5^+	$^1A_1'$: $1a_1'^2, 1e_1'^4, 1e_2'^4, 1a_2''^2, 2a_1'^2$	D_{5h}	2.94	1	1
B_5^0	$^1A_1$: $1a_1^2, 1b_2^2, 2a_1^2, 3a_1^2, 1b_1^2, 2b_2^2, 4a_1^2, 3b_2^1$	C_{2V}	2.34	0	1
$B_4^{(2-)}$	^1A_g:$1a_{1g}^2, 1e_u^4, 1b_{1g}^2, 1b_{2g}^2, 2a_{1g}^2, 11a_{2u}^2$	D_{4h}	2.78	1	2
B_4^0	^1A_g: $1a_g^2, 1b_{1u}^2, 1b_{2u}^2, 1b_{3g}^2, 1b_{3u}^2,, 2a_g^2$	D_{2h}	3.08	1	1
B_3^+	$^1A_1'$: $1a_1'^2, 1e'^4, 1a_2''^2$	D_{3h}	0.77	0	1

2c–2e boron bonds. The HOMO ($1a_1'^2$) and HOMO-1 ($1a_2''^2$) are σ-MO and π-MO, respectively, therefore they make the B_5^+ doubly (σ- & π-) aromatic and this aromaticity replace itself in the high first singlet excitation energy (Table 3). Now it can be understood why B_5^+ is a wonderful cluster in CID or "collision induced dissociation" [25–31]. $D_{5h}(^1A_1)$ distortion might be explained through the SOJT, because of non-occupied MOs of related pentagon structure, where indicates a deviation from up symmetry which is similar to the distortion of the B_4 clusters into rhombus.

B_5^- cluster can be predicted with starting of the B_5^+ cluster. The $1e_1''^2$-LUMO in B_5^+ $D_{5h}(^1A_1)$ MOs is a doubly degenerate and anti-bonding/bonding orbital related to the HOMO-1 ($1a_2''^2$) π-MO. Occupation of one of doubly degenerate LUMO via $2e^-$ can be distorted the D_{5h} to the C_{2v} structures due to the JT effect. This calculation have exhibited $C_{2v}(^1A_1$: $1a_1^2, 1b_2^2, 2a_1^2, 3a_1^2, 1b_1^2, 2b_2^2, 4a_1^2, 1a_2^2$) MO with 50.5 (B3LYP/6-311+G*) kcal/mol higher than the global minimum and it is a first order saddle point. The $2e_1'^4$-LUMO + 1 has been occupied instead of $1e_1''^4$-LUMO. The singlet $D_{5h}(1a_1'^2, 1e_1'^4, 1e_2'^4, 1a_2''^2, 2a_1'^2, 1e_1''^2)$ electronic configuration of B_5^- should also lead to the JT distortion. Therefore, the $C_{2v}(^1A_1$:$1a_1^2, 1b_2^2, 2a_1^2, 3a_1^2, 1b_1^2, 2b_2^2, 4a_1^2, 3b_2^2$) planar is the B_5^- global minimum position. B_5^-, have $4e^-$ on globally σ-delocalized $4a_1$-HOMO-1 and $3b_2$-HOMO and also $2e^-$ on globally delocalized 1b1-HOMO-3 that appears a conflicting aromaticity system (σ-antiaromatic and π-aromatic).

In $B_5^{(0)}$, due to the JT effect any occupation of a doubly degenerate LUMO via any e^- can be distorted D_{5h} point group to the C_{2v} structures. In addition, the $2e_1'^4$-LUMO + 1 has been occupied instead of $1e_1''^4$-LUMO and also the singlet D_{5h} $(1a_1'^2, 1e_1'^4, 1e_2'^4, 1a_2''^2, 2a_1'^2, 1e_1''^1)$ configuration of $B_5^{(0)}$ can lead to the JT distortion.

Therefore, the $C_{2v}(^1A_1$:$1a_1^2, 1b_2^2, 2a_1^2, 3a_1^2, 1b_1^2, 2b_2^2, 4a_1^2, 3b_2^1$)) planar is the $B_5^{(0)}$ global minimum position. Herein, $B_5^{(0)}$ has $4e^-$ on globally σ-delocalized $4a_1$-HOMO-1 and $3b_2$-HOMO including one e^- on globally delocalized 1b1-HOMO-3 that appears a conflicting aromaticity system (σ-antiaromatic and π-aromatic) but lower than the B_5^-. NBO analysis and experimentally investigating of the photoelectron

study [9, 19, 21–24] confirmed our $B_5^{0\mp1}$ model by this work.

Due to the geometric structure of (σ-antiaromatic and π-aromatic) B_5^- has lower symmetry which means antiaromaticity can destroyed the aromaticity towards a net antiaromaticity position. B_6^{+2} di-cation has sixteen electrons in valance with 6 peripheral $2c$–$2e$ B–B bonds out of HOMO-2 ($1b_{2u}$), HOMO-3 ($1e_{2g}^4$), HOMO-4 ($1e_{1u}^4$), and HOMO-5 ($1a_{1g}$), while 4 electrons are located on 2 MOs and both of them are bonding ($2a_{1g}$-σ-HOMO and $1a_{2u}$-π-HOMO-1). Therefore, B_6^{+2} is a doubly aromatic and our calculation exhibits that it belongs to the D_{6h} ($1A_{1g}$) point group and has a minimum at several levels of theory (B3LYP/6-311+G*, MP2/6-311+G*, and CCSD (T)/6-311+G*).

$B_6^{(0)}$ cluster has a special pentagonal-pyramid electronic structure corresponds to a global minimum [47] where the planar pentagonal is included of one boron atom at the center among the five-remain boron atoms in the ring. It is not a minimum global because of a small cavity inside of the pentagon. The tightest optimization exhibit that the global minimum structure of $\mathbf{B}_6^{(0)}$ is the pyramid C_{5v} ($^1A_1$: $1a_1^2$, $1e_1^4$, $2a_1^2$, $1e_2^4$, $3a_1^2$, $2e_1^4$) electronic configuration with the boron atom located 0.955 Å above the center of the pentagon ring (Table 1). The triplet C_{2h}(^{3}Au: $1a_g^2$, $1b_u^2$, $2a_g^2$, $2b_u^2$, $3a_g^2$, $1a_u^2$, $3b_u^2$, $4a_g^2$, $4b_u^1$, $1b_g^1$) and also the singlet C_2(^1A: $1a^2$, $1b^2$, $2b^2$, $2a^2$, $3a^2$, $4a^2$, $3b^2$, $5a^2$ $4b^2$) from the cyclic B_6 geometry obey the JT distortion with 7.3 and 8.1 kcal/mol (CCSD(T)/6-311+G(2df)//B3LYP/6-311 · G*), respectively higher in energy [21–23, 28]. Based on D_{5h}($^1A_1'$: $1a_1'^2$, $1e_1'^4$, $1a_2''^2$, $1e_2'^4$, $2a_1'^2$, $2e_1'^4$), the MOs are $1e_2'^4$-HOMO-2, $1e_1'^4$-HOMO-4, and $1a_1'^2$-HOMO-2 that are located into $2c$–$2e$ B–B bonds with a peripheral bonding and $1a_2''^2$-HOMO-3 which is appeared via $2p_z$ atomic orbitals for creating the global-bonding. The $2e_1'^4$-HOMO and $2a_1'^2$-HOMO-1 are organized from $2p$-radial atomic orbitals to create the global-bonding in the $B_6^{(0)}$. This ion is a doubly σ&π-aromatic.

$B_6^{(2-)}$, formed by two extra electrons compared to $B_6^{(0)}$, with a planar electronic structure by D_{2h} point group (^1A_g: $1a_g^2$, $1b_{1u}^2$, $2a_g^2$, $1b_{2u}^2$, $1b_{3g}^2$, $1b_{3u}^2$, $3a_g^2$, $2b_{2u}^2$, $2b_{1u}^2$, $1b_{2g}^2$) in the global minimum position [47]. This configuration is extracted from the D_{6h} hexagon that obeys of the first order JT distortion. Six MOs including $2b_{2u}^2$-HOMO-2, $1b_{3g}^2$-HOMO-5 $1b_{2u}^2$-HOMO-6, $2a_g^2$-HOMO-7, $1b_{1u}^2$-HOMO-8, and $1a_g^2$-HOMO-9 are localized into six $2c$–$2e$ B–B bonds; therefore they make the peripheral bonding. The other MOs (four orbitals) make the global bonding in this cluster. The $2b_{1u}^2$-HOMO-1 and $3a_g^2$-HOMO-3 produce σ-radial molecular orbitals which are pure bonding, and the $2b_{1u}^2$-HOMO-1 being relatively anti-bonding. Therefore, $B_6^{(2-)}$ anion has two globally de-localized orbital molecules, which produce an anti-aromatic situation. The remaining delocalized orbitals are $1b_{3u}^2$-HOMO-4 (completely bonding) and $1b_{2g}^2$-HOMO (partially bonding). Since this anion has 4σ and 4π e^-on the globally delocalized orbitals and also six $2c$–$2e$ peripheral B–B bonds, it has a doubly (σ & π) anti-aromatic situation.

NBO Analysis

Via NBO approach the electron delocalization is interpreted based on Lewis information. Obviously, the charge in the Lewis orbital has shown a low amount of electronic charge due to strong effects of electron delocalization. In an orbital resonance, the major and minor contribution among the atomic orbitals can be estimated through several calculations. Due to perturbation phenomenon, some operators such as Fock-Matrix, the donor–acceptors of bonding & anti-bonding interactions the NBO evaluation has been calculated and are listed in Table 4.

As it can be seen in Table 1, all bonds in $B_6^{(2+)}$ are completely equal and wave function, occupancy, deviation (in both hybrids), and "θ" are identical due to D_{6h} ($^1A_{1g}$) structure, which has a minimum energy at several levels of calculations. This kind analyzing are accomplished via examining all possible interactions among donor Lewis-types (Field orbitals) with acceptors (empty orbitals) non-Lewis of NBOs. For donor orbitals with index (i) and acceptor orbitals with index (j), the stabilization energies $E(2)$ completely associated with delocalization. The equation as follows exhibits the relation of F Matrix as: $E(2) = \Delta E_{ij} = q_i \frac{F_{i,j}^2}{\varepsilon_j - \varepsilon_i}$, where q_i are the donor occupancies and $\varepsilon_j - \varepsilon_i$ are diagonal orbital energies. In addition $F_{i,j}^2$ is the Fock-matrix function (Table 4).

Based on NBO analysis (Tables 4, 5), NHO direction and bond bending (Deviations from line of nuclear centers) can be estimated for understanding the situation of π and σ orbitals. These data often are useful for predication the direction of geometry changing results from geometries optimization. The

Table 4. Donor and acceptor analysis

Donor NBO(*i*)	Acceptor NBO (*j*)	*E*(2), kcal/mol	*E*(*j*) − *E*(*i*), a.u.	*F* (*i*, *j*), a.u.
		$B_6^{(2+)}$		
B1–B2 (σ)	LP(1) B2	0.91	0.49	0.021
B2–B3 (σ)	LP (1) B3	4.00	0.49	0.043
B3–B4 (σ)	LP (1) B4	4.00	0.49	0.043
B4–B5 (σ)	LP(1) B5	0.91	0.49	0.021
B5–B6 (σ)	LP(1) B6	0.91	0.49	0.021
B6–B1 (σ)	LP(1) B1	4.00	0.49	0.043
		$B_6^{(2-)}$		
B1–B2 (σ)	LP*(2) B2	33.29	0.45	0.126
B1–B3 (σ)	LP* (2) B3	48.01	0.45	0.151
B2–B4 (σ)	LP (1) B4	7.20	0.80	0.069
B4–B5 (σ)	LP(1) B5	1.39	0.82	0.031
B5–B6 (σ)	LP(1) B6	9.48	0.50	0.073
		$B_6^{(0)}$		
B1–B2 (σ)	LP*(2) B2	33.29	0.45	0.126
B1–B3 (σ)	LP* (2) B3	48.01	0.45	0.151
B1–B4 (σ)	LP (1) B4	7.20	0.80	0.069
B1–B5 (σ)	LP(1) B5	1.39	0.82	0.031
B1–B6 (σ)	LP(1) B6	9.48	0.50	0.073

direction of a hybrid is specified in terms of the polar (θ) and azimuthal (φ) angles of the vector describing its *p*-component. The hybrids directions are then compared with those direction of the lines of the centers between two nuclei for determining the bending of those bonds, expressed as the deviation angles between these two directions. For $B_6^{(2+)}$, $B_6^{(2-)}$ and $B_6^{(0)}$ NBO calculations exhibit that these structures are the dominant Lewis structure. However, based on advanced valance bond theory, covalent-ionic resonances are not necessary due to the inclusion of bond-polarity effects in a resonance structure. By this work, for each NAO functions, core, valence, or Rydberg, the orbital occupancy and the orbital energy are shown and it is notable that the occupancies of the Rydberg (Ryd) NAOs are typically much lower than those of the core and valence (Val) NAOs of the natural minimum basis (NMB) set.

In addition, the occupancies for a enough approximation, Lewis and non-Lewis NBOs, population, core number(CR), two-center bond (BD), three-center bond (3C), and lone pairs (LP) NBOs, Lewis—low-occupancy (L) and Non-Lewis high-occupancy (NL), and also the optimum deviation (Dev) of any formal bond order have been considered for $B_5^{(+)}$, $B_5^{(-)}$, $B_5^{(0)}$, $B_4^{(2+)}$, $B_4^{(2-)}$, $B_4^{(0)}$, $B_3^{(0)}$, $B_3^{(+)}$ and $B_3^{(-)}$.

The calculations of Natural Population including charges, Rydberg, core and valance for several variants of $B_6^{0,\mp2}$ are listed in Table 6. Since the bonds order are the integer number of chemical bonds, in molecules which have resonance or non-classical bonding, bond order may not be an integer. In other words, the delocalized molecular orbitals contain π orbitals essentially yielding half of the π together with half of the σ https://en.wikipedia.org/wiki/Sigma_bond bonds for each pair of atoms. Electron localization function (ELF) and Localized orbital localization (LOL) analysis that has been investigated by Beck and coworkers [48] illustrated a spherically average like-spin pair including suitable correlation with considering the Fermi hole. So, by this introducing, a new function as "electrons localization functions" appears for any further discussion and calculation in the physical sciences as known (ELF).

$$\mathrm{ELE}(r) = \frac{1}{1 + [D(r)/D_{0(r)}]^2}, \quad (1)$$

where

$$D(r) = \frac{1}{2}\sum_i \eta_i |\nabla\varphi_i|^2 - \frac{1}{8}\left[\frac{|\nabla\rho_\alpha|^2}{\rho_\alpha(r)} + \frac{|\nabla\rho_\beta|^2}{\beta(r)}\right], \quad (2)$$

and

Table 5. Natural hybrid orbitals (NHO) direction and bond bending deviations from line of nuclear centers in variants of $B_6^{0,\mp2}$

Line of center		Hybride 1			Hybride 2			Wave function	OCC
θ	φ	θ	φ	Dev	θ	φ	Dev	B_i–B_j bonding	
					$B_6^{(0)}$				
73.9	212.8	89.3	274.4	62.6	97.3	343.6	48.9	$0.711SP^{1.02}$ of B1 + 0.702 $SP^{1.58}$ of B2	1.939
74.0	147.1	89.7	85.7	62.6	97.6	16.4	48.8	0. 712 $P^{1.01}$ of B1 + 0.701 $P^{1.59}$ of B4	1.939
108.3	180.0	101.8	208.8	28.5	78.2	331.2	28.5	0.707 $P^{1.37}$ of B2 + 0.707 $P^{1.37}$ of B3	1.966
73.9	147.2	82.7	196.4	48.9	90.7	265.6	62.6	$0.702SP^{1.58}$ of B3 + 0.711 $SP^{1.02}$of B4	1.939
106.0	32.9	90.3	94.4	62.6	82.4	163.6	48.8	$0.712SP^{1.01}$ of B4 + 0.707 $SP^{1.36}$ of B6	1.939
108.2	180.0	101.6	151.2	28.6	78.4	28.8	28.6	$0.707SP^{1.36}$ of B5 + 0.707 $SP^{1.36}$ of B6	1.967
					$B_6^{(2-)}$				
90.0	145.1	90.0	104.3	40.9	90.0	17.6	52.5	$0.692SP^{1.11}$ of B1 + 0.721 $SP^{1.61}$ of B2	1.889
90.0	180.0	90.0	0.0	180.0	90.0	180.0	180.0	$0.711SP^{1.02}$ of B1 + 0.702 $SP^{1.58}$of B2	1.947
90.0*	180.0	90.0	0.0	180.0	90.0	180.0	180.0	0. 707 $P^{19.2}$ of B1 + 0.707 $P^{19.2}$ of B4	1.415
90.0	214.9	90.0	255.7	40.9	90.0	342.4	52.4	$0.692SP^{1.11}$ of B1 + 0.721 $SP^{1.61}$ of B5	1.889
90.0	180.0	90.0	149.0	31.0	90.0	31.0	31.0	$0.707SP^{1.48}$ of B2 + 0.707 $SP^{1.48}$ of B3	1.983
90.0	214.9	90.0	162.4	52.4	90.0	75.7	40.9	$0.721SP^{1.01}$ of B3 + 0.692 $SP^{1.36}$ of B4	1.889
90.0	325.1	90.0	284.3	40.9	90.0	197.6	52.4	$0.692SP^{1.11}$ of B4 + 0.721 $SP^{1.61}$ of B6	1.889
					$B_6^{(2+)}$				
90.0	283.8	90.0	306.6	22.8	90.0	81.1	22.8	$0.707SP^{1.05}$ of B1 + 0.707 $SP^{1.05}$of B2	1.980
90.0	163.8	90.0	141.1	22.8	90.0	6.6	22.8	$0.707SP^{1.05}$ of B1 + 0.707 $SP^{1.05}$of B6	1.980
90.0	223.8	90.0	246.6	22.8	90.0	21.0	22.8	$0.707SP^{1.05}$ of B2 + 0.707 $SP^{1.05}$ of B3	1.9800
90.0	163.8	90.0	186.6	22.8	90.0	321.1	22.8	$0.707SP^{1.05}$ of B3 + 0.707 $SP^{1.05}$ of B4	1.9800
90.0	103.8	90.0	126.6	22.8	90.0	261.1	22.8	$0.707SP^{1.05}$ of B4 + 0.707 $SP^{1.05}$of B5	1.9800
90.0	43.8	90.0	66.6	22.8	90.0	201.0	22.8	$0.707SP^{1.05}$ of B5 + 0.707 $SP^{1.05}$ of B6	1.9800

$$D_{0(r)} = \frac{3}{10}(6\pi^2)^{2/3}[\rho_\alpha(r)^{5/3} + \rho_\beta(r)^{5/3}], \quad (3)$$

for closed-shell systems, since $\rho_\alpha(r) = \rho_\beta(r) = \frac{1}{2}\rho$, D and D_0 terms can be simplified as

$$D(r) = \frac{1}{2}\sum_i \eta_i |\nabla\varphi_i|^2 - \frac{1}{8}\left[\frac{|\nabla\rho|^2}{\rho(r)}\right], \quad (4)$$

and

$$D_{0(r)} = \frac{3}{10}(3\pi^2)^{2/3}\rho(r)^{5/3}. \quad (4)$$

Savin et al. [49] indicated that $D(r)$ determines the excess kinetic energies due to the Pauli repulsion, while $D_0(r)$ is known as Thomas–Fermi kinetic energies term. In other words they re-considered the ELF in view point of kinetic energy through Kohn–Sham DFT's wave-function. Therefore, ELF would be in the range of [0, 1] and a large ELF value indicates that electrons are strongly localized.

ELF is a strong factor that is useful for many varieties of molecules in organic and inorganic compounds and also especially for cluster rings of Boron Nitride molecules. Localized orbital locator (LOL) is the other function similar ELF that has been investigated by Becke and coworkers [50].

$$\mathrm{LOL}(r) = \frac{\tau(r)}{1 + \tau(r)},$$

where

$$(r) = \frac{D_0(r)}{\frac{1}{2}\sum_i \eta_i |\nabla\varphi_1|^2}. \quad (5)$$

In equation (6), $D_0(r)$ for both spin-polarized and closed-shell systems are explained in the same mean-

Table 6. Summary of natural population analysis

Natural		Natural Population			
atom No.	charge	core	valence	rydberg	total charge
		B_6^{2-}			
1	–0.50587	1.99628	3.49179	0.01780	5.50587
2	–0.24707	1.99765	3.23021	0.01921	5.24707
3	–0.24706	1.99765	3.23020	0.01921	5.24706
4	–0.50587	1.99628	3.49179	0.01780	5.50587
5	–0.24707	1.99765	3.23021	0.01921	5.24707
6	–0.24707	1.99765	3.23022	0.01921	5.24707
		B_6^{2+}			
1	0.33331	1.99726	2.66024	0.00919	4.66669
2	0.33346	1.99726	2.66009	0.00919	4.66654
3	0.33323	1.99726	2.66032	0.00919	4.66677
4	0.33331	1.99726	2.66023	0.00919	4.66669
5	0.33345	1.99726	2.66010	0.00919	0.00919
6	0.33324	1.99726	2.66031	0.00919	4.66676
		B_6^0			
1	0.05700	1.99671	2.93447	0.01182	4.94300
2	0.05764	1.99671	1.99671	2.93384	0.01181
3	1.99671	1.99671	2.93424	0.01182	4.94277
4	0.05730	1.99671	2.93418	0.01182	4.94270
5	0.05764	1.99671	2.93384	0.01181	4.94236
6	–0.28681	1.99613	3.26351	0.02717	5.28681

Molecule	Total Lewis	Valence non-Lewis	Rydberg non-Lewis
$B_6^{(2-)}$	26.05020 (81.4069%)	5.88689 (18.3965%)	0.06291 (0.1966%)
$B_6^{(2+)}$	24.55640 (87.7014%)	3.41292 (12.1890%)	0.03068 (0.1096%)
B_6^0	26.79950 (89.3317%)	3.15753 (10.5251%)	0.04297 (0.1432%)

ing as in ELF. Jacobsen exhibited that LOL supply more definitive and obvious image than ELF therefore LOL can be interpreted in kinetic energies way better as for ELF; as regards LOL can also be interpreted in viewpoint of localized orbital. Region data area of LOL is same as ELF, which means are placed between zero and one [0, 1]. The electron densities, values of orbitals and LUMO, HOMO orbitals, electrons spin densities, electrostatic charges, ELF, LOL and total electrostatic potential (ESP) using the Multifunctional Wave-function analyzer have also been calculated in this work [51].

DISCUSSION

In this work we exhibit some boron clusters can be doubly (σ- and π-) aromatic such as B_3^-, B_4^{2+}, B_5^+, and even B_7^+, and also some other clusters can be globally doubly anti-aromatic, such as, B_6^{2-}. Anti-aromatic molecules might be interpreted in terms of formation of areas of island aromatic position [52, 53]. In the B_6^{2-} clusters, the globally delocalized σ- and π electrons can be localized over two areas composed of three boron atoms. Several clusters may have conflicting aromaticity, such as B_5^- (which is π-aromatic and σ-anti-aromatic). In addition to peripheral $2c$–$2e$ B–B bonds globally delocalized π-MOs, and globally delocalized σ-Mos. It is important to mention that there is good similarity between the planar boron clusters with $4n$ π electrons to anti-aromatic. By this work can be exhibited that a globally π-anti-aromatic molecule such as B_6^{2-} could have islands of π-aromaticity. For explaining low symmetry (D_{2h} instead of D_{6h}) of

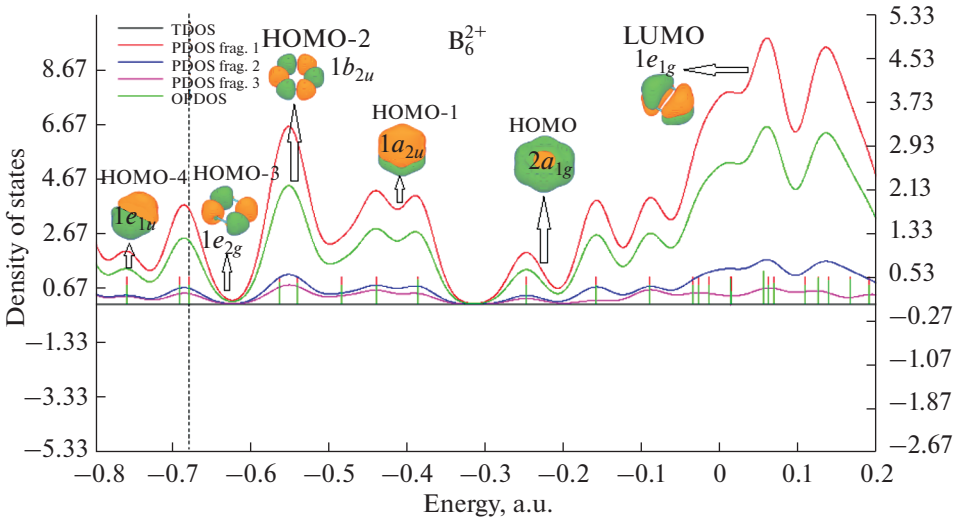

Fig. 2. TDOS, PDOS and OPDOS plots versus molecular orbital energies of B_6^{2+} (D_{6h}, $^1A_{1g}$) including $1e_{1u}$, $1e_{2g}$, $1b_{2u}$ $1a_{2u}$, and $2a_{1g}$ of HOMO-4, HOMO-3, HOMO-2, HOMO-1, HOMO and LUMO, respectively.

B_6^{2-}, it is needed to consider this cluster as being globally π-anti-aromatic. For B_5^- also the high TRE cannot explain the low symmetry (C_{2v} instead of D_{5h}) as well as the small first singlet vertical excitation energy. Since the global σ-anti-aromaticity in the B_5^- cluster is recognized, the low symmetry C_{2v} structure and small first singlet vertical excitation energy has rather simple explanation, which is not able to explain only π-aromatic situation in this type of clusters. Suitable geometric and optimization is an essential factor, which determines the shape of the most stable structures.

In addition, plotting Total/Partial/Overlap population density-of-states (TDOS, PDOS, OPDOS), have been done for all components of $B_n^{\mp,0}$ clusters. The original total DOS (TDOS) of isolated $B_n^{\mp,0}$ (n = 6–10) clusters can be written as $\mathrm{TDS}(E) = \sum_i \delta(E - \varepsilon_i)$ where ε_i is eigenvalue of particle Hamilton and δ is Dirac delta function. By replacing δ with a function such as Gaussian, Lorentzian and pseudo-Voigt function, broadened TDOS can be yielded. The normalized Gaussian function is defined as $G(x) = \frac{1}{C\sqrt{2\pi}} e^{-\frac{x^2}{2c^2}}$ where $= \frac{FWHM}{2\sqrt{2}\sqrt{\ln 2}}$. This parameter is acronym of "full width at half maximum," it is an adjustable parameter in Multiwfn, the larger FWHM the TDOS graph looks smoother and analysis is easier to perform, but more fine-structure is masked. Here the Lorentzian function can be defined as $L(x) = \frac{FWHM}{2\pi} \frac{1}{x^2 + 0.25FWHM^2}$. Pseudo-Voigt function is weighted linear combination of Gaussian and Lorentzian functions: $P(X) = w_{\mathrm{gauss}} G(x) + (1 - w_{\mathrm{gauss}}) L(x)$. Obviously, if $G(x)$ and $L(x)$ are normalized, normalization condition for $P(x)$ always holds regardless of the select of w_{gauss}. PDOS function of fragment A is defined as $\mathrm{PDOS}_A(E) = \sum_i \Xi_{i,A} F(E - \varepsilon_i)$, where $\Xi_{i,A}$ is the composition of fragment A in orbital i. The OPDOS for A and B fragments is formulated as $\mathrm{OPDOS}_{(A,B)}(E) = \sum_i^j X_{A,B} F(E - \varepsilon_i)$, where $X_{A,B}^i$ is the composition of total cross term between fragment A and B in orbital i. However if the discrete lines are broadened, from the height of black curve (TDOS) we can clearly know how dense the energy levels are distributed everywhere. Besides, TDOS, PDOS and OPDOS clearly identify characters of each orbital by observing these curves (Figs. 2–4).

The red curve is high in the region of –0.8 to +0.2 a.u., so we can be concluded that 2p atomic orbitals of boron atoms have significant contribution to corresponding MOs. Since the green curve is greater than the other forms, denote corresponding MOs are favorable or unfavorable for forming chemical bond between boron 2p orbitals together, it is shown that the orbital pointed by the leftmost arrow is very helpful for bonding, while the high-energy state orbitals (>0.2 a.u.) are not conducive for bonding (namely anti-bonding character), fortunately they haven't been occupied, otherwise the molecule must be broken. Finally, it can be mentioned this information for Boron clusters are useful for any further research in boron properties in industrial, drug design and agricultures activities [54–56].

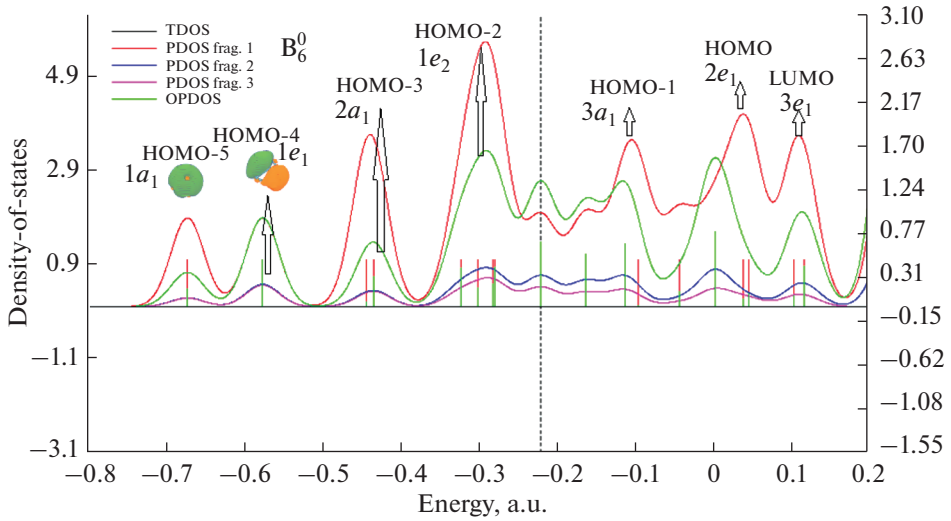

Fig. 3. TDOS, PDOS and OPDOS plots versus molecular orbital energies of B_6^0 (C_{5v}, $^1A_1$) including $1a_1$, $1e_1$, $2a_1$, $1e_2$, $3a_1$, $2e_1$ and $3e_1$ of HOMO-5, HOMO-4, HOMO-3, HOMO-2, HOMO-1, HOMO and LUMO, respectively.

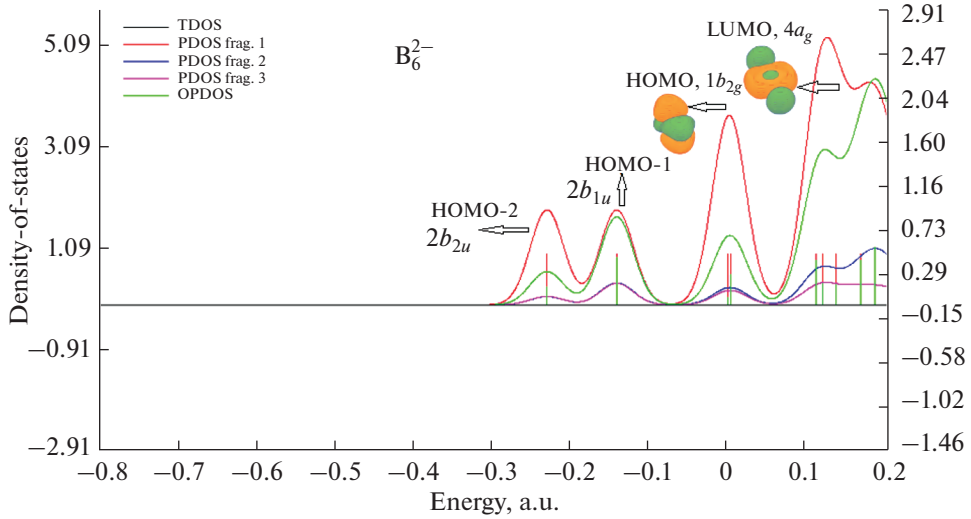

Fig. 4. TDOS, PDOS and OPDOS plots versus molecular orbital energies of B_6^0 B_6^{2-} (D_{2h}, ^1A_g) including $4a_g$, $1b_{2g}$, $2b_{1u}$ and $2b_{2u}$ of LUMO, HOMO, HOMO-1, HOMO-2, respectively.

CONCLUSIONS

On the fundamental of NBO bonding analysis performed for $B_n^{\mp,0}$ clusters, which have been discussed about the next chemical bonding model for planar or quasi-planar in viewpoint of the second order Jahn–Teller effects (SOJT). The number of $2c$–$2e$ peripheral in planar or quasi-form the clusters are equal to the number of peripheral forms. In addition, there is delocalization – MOs, which make the cluster aromatic for $4n + 2$ π electrons and in other hand or for 4nπ electrons have an anti-aromatic position. There is delocalization of σ-MOs, which make the cluster globally σ-aromatic for $4n + 2$ σand for $4n$ σ electrons make it anti-aromatic.

ACKNOWLEDGMENTS

The Author thanks Islamic Azad University for providing computer equipment.

CONFLICT OF INTEREST

The authors declare that they have no conflicts of interest.

REFERENCES

1. D. Sundholm, R. J. F. Berger, and H. Fliegl, Phys. Chem. Chem. Phys. **18**, 15934 (2016). https://doi.org/10.1039/C6CP01968D
2. E. Steiner and P. W. Fowler, J. Phys. Chem. A, **105**, 9553 (2001). https://doi.org/10.1021/jp011955m
3. E. Steiner, P. W. Fowler, and R. W. A. Havenith, J. Phys. Chem. A **106**, 7048 (2002). https://doi.org/10.1021/ja015952z
4. Z. Chen, C. S. Wannere, C. Corminboeuf, et al., Chem. Rev. **106**, 3842 (2005). https://doi.org/10.1021/cr030088
5. Z. X. Wang and P. V. R. Schleyer, Science **292**, 2465 (2001). https://doi.org/10.1126/science.1060000
6. H. Tanaka, S. Neukermans, E. Janssens, et al., J. Am. Chem. Soc. **125**, 2863(2003). https://doi.org/10.1021/ja029157c
7. C. A. Tsipis, Coord. Chem. Rev. **249**, 2740 (2005). https://doi.org/10.1016/j.ccr.2005.01.031
8. E. D. Jemmis and E. G. Jayasree, Acc. Chem. Res. **36**, 816 (2003). https://doi.org/10.1021/ar0300266
9. J. Juselius, M. Straka, and D. Sundholm, J. Phys. Chem. A **105**, 43, 9939 (2001). https://doi.org/10.1021/jp012346h
10. Y. C. Lin, D. Sundholm, J. Juselius, et al., J. Phys. Chem. A **110**, 4244 (2006).
11. C. G. Zhan, F. Zheng, and D. A. Dixon, J. Am. Chem. Soc. **124**, 147 (2002).
12. J. C. Santos, J. Andres, A. Aizman, et al., J. Chem. Theory Comp. **1**, 83 (2005). https://doi.org/10.1021/ct0499276
13. A. Datta and S. K. Pati, J. Phys Chem. A **108**, 9527, (2004). https://doi.org/10.1021/jp047204c
14. R. W. A. Havenith, P.W. Fowler, E. Steiner, et al., Phys. Chem. Chem. Phys. **6**, 285 (2004)
15. X. B. Hu, H. R. Li, W. C. Liang, et al., Chem. Phys. Lett. **426**, 39 (2006). https://doi.org/10.1016/j.cplett.2006.05.103
16. X. Hu, H. Li, W. Liang, et al., Chem. Phys. Lett. **402**, 539 (2005). https://doi.org/10.1016/j.cplett.2004.12.106
17. X. W. Hu, H. R. Li, W. C. Liang, et al., New J. Chem. **29**, 1295 (2005). https://doi.org/10.1039/B507592K
18. F. F. Wang, Z. R. Li, D. Wu, X et al., Chem. Phys. Chem. **7**, 1136 (2006). https://doi.org/10.1002/cphc.200600014
19. H. J. Zhai, L. S. Wang, A. N. Alexandrova, et al., J. Phys. Chem. A **107**, 9319 (2003). https://doi.org/10.1021/jp0357119
20. A. E. Kuznetsov and A. I. Boldyrev, Struct. Chem. **13**, 141 (2002). https://doi.org/10.1023/A:1015704515336
21. H. J. Zhai and L. S. Wang, J. Chem. Phys. **117**, 7917 (2002). https://doi.org/10.1063/1.1511184
22. A. N. Alexandrova, A. I. Boldyrev, H. J. Zhai, et al., J. Chem. Phys. **122**, 054313 (2005). https://doi.org/10.1063/1.1839575
23. A. N. Alexandrova, E. Koyle, and A. I. Boldyrev, J. Mol. Mod. **12**, 569 (2006). https://doi.org/10.1007/s00894-005-0035-5
24. H. J. Zhai, L. S. Wang, D. Zubarev, et al., J. Phys. Chem. A, **110**, 1689 (2006). https://doi.org/10.1021/jp0559074
25. L. Hanley and S. L. Anderson, J. Phys. Chem. **91**, 5161 (1987). https://doi.org/10.1021/j100304a007
26. L. Hanley and S. L. Anderson, J. Chem. Phys. **89**, 2848 (1988). https://doi.org/10.1063/1.454989
27. L. Hanley, J. L. Whitten, and S. L. Anderson, J. Phys. Chem. **92**, 5803 (1988). https://doi.org/10.1021/j100331a052
28. A. N. Alexandrova, H. J. Zhai, L. S. Wang, et al., Inorg Chem. **43**, 3588 (2004). https://doi.org/10.1021/ic049835r
29. K. Y. Zhizhin, V. N. Mustyatsa, E. Y. Matveev, et al., Russ. J. Inorg. Chem. **48**, 671 (2003).
30. K. Yu. Zhizhin, V. N. Mustyatsa, E. A. Malinina, et al., Russ. J. Inorg. Chem. **49**, 180 (2004).
31. A. P. Zhdanov, V. M. Retivov, G. A. Razgonyaeva, et al., Russ. J. Inorg. Chem. **60**, 771 (2015). https://doi.org/10.1134/S0036023615070189
32. R. Kawai and J. H. Weare, J. Chem. Phys. **95**, 1151(1991). https://doi.org/10.1063/1.461145
33. S. J. La Placa, P. A. Roland, et al., J. Chem. Phys. Lett. **190**, 163 (1992). https://doi.org/10.1016/0009-2614(92)85319-6
34. V. V. Avdeeva, E. A. Malinina, and N. T. Kuznetsov, Russ. J. Inorg. Chem. **62**, 1673 (2017). https://doi.org/10.1134/S0036023617130022
35. K. Yu. Zhizhin, A. P. Zhdanov, and N. T. Kuznetsov, Russ. J. Inorg. Chem. **55**, 14, 2089 (2010)
36. H. Kato, K. Yamashita, and K. Morokuma, Chem. Phys. Lett. **190**, 361 (1992). https://doi.org/10.1016/0009-2614(92)85352-B
37. P. A. Roland and J. J. Wynne, J. Chem. Phys **99**, 8599 (1993). https://doi.org/10.1063/1.465583
38. H. Kato, K. Yamashita, and K. Morokuma, Bull. Chem. Soc. Jpn. **66**, 3358 (1993). https://doi.org/10.1246/bcsj.66.3358
39. I. Boustani, Int J. Quantum Chem. **52**, 1081 (1994). https://doi.org/10.1002/qua560520432
40. I. Boustani, Chem. Phys. Lett. **240**, 135(1995). https://doi.org/10.1016/0009-2614(95)00510-B
41. K. Yu. Zhizhin, N. N. Mal'tseva, A. Yu. Bykov, and N. T. Kuznetsov, Russ. J. Inorg. Chem. **55**, 2128 (2010)
42. I. Boustani, Phys. Rev. B **55**, 16426 (1997). https://doi.org/10.1103/PhysRevB.55.16426
43. J. Aihara, H. Kanno, and T. Ishida, J. Am Chem. Soc. **127**, 38, 13324 (2005). https://doi.org/10.1021/ja053171i

44. M. Monajjemi, V. S. Lee, M. Khaleghian, et al, J. Phys. Chem. C **114,** 15315, (2010) https://doi.org/10.1021/jp104274z

45. T. Lu and F. A. Chen, J. Comp. Chem. **33**, 580 (2012).

46. M. Monajjemi, Theor. Chem. Acc. **134**, 77 (2015). https://doi.org/10.1007/s00214-015-1668-9

47. A. Alexandrova, A. Boldyrev, H.-Jin Zhai, and L. S. Wang, Coord. Chem. Rev. **250**, 2811 (2006). https://doi.org/10.1016/J.CCR.2006.03.032

48. A. D. Becke and K. E. Edgecombe, J. Chem. Phys. **92**, 5397 (1990). https://doi.org/10.1063/1.458517

49. A. Savin, J. Mol. Struct.: THEOCHEM **727**, 127 (2005) https://doi.org/10.1016/j.theochem.2005.02.034

50. A. D. Becke, J. Mol. Struct.: THEOCHEM **51**, 527 (2000).

51. T. Lu and F. Chen, J. Mol. Graph. Model **38**, 314 (2012).

52. A. N. Alexandrova, A. Boldyrev. H. J. Zhai, et al, J. Phys. Chem. A **107**, 1359 (2003). https://doi.org/10.1021/jp0268866

53. E. A. Malinina, V. V. Avdeeva, L. V. Goeva, et al., Russ. J. Inorg. Chem. **55**, 2148 (2010). https://doi.org/10.1134/S0036023610140032

54. M. Brdar-Jokanović, Int. J. Mol. Sci. **21**, 1424 (2020). https://doi.org/10.3390/ijms21041424

55. D. H. Lewis, New Phytol. **221**, 1685 (2019).

56. K. Chakrabarty, W. C. Chen, P. A. Baker, et al., Materials **13**, 3622 (2020). https://doi.org/10.3390/ma13163622